

ARTICLE



CEND1 deficiency induces mitochondrial dysfunction and cognitive impairment in Alzheimer's disease

Wenting Xie^{1,4}, Dong Guo^{1,4}, Jieyin Li^{1,4}, Lei Yue², Qi Kang¹, Guimiao Chen¹, Tingwen Zhou¹, Han Wang¹, Kai Zhuang¹, Lige Leng¹, Huifang Li¹, Zhenyi Chen³, Weiwei Gao² and Jie Zhang^{1,2,3}

© The Author(s), under exclusive licence to ADMC Associazione Differenziamento e Morte Cellulare 2022

Alzheimer's disease (AD) is the most common form of neurodegenerative disease featured with memory loss and cognitive function impairments. Chronic mitochondrial stress is a vital pathogenic factor for AD and finally leads to massive neuronal death. However, the underlying mechanism is unclear. By proteomic analysis, we identified a new mitochondrial protein, cell-cycle exit and neuronal differentiation 1 (CEND1), which was decreased significantly in the brain of 5xFAD mice. CEND1 is a neuronal specific protein and locates in the presynaptic mitochondria. Depletion of CEND1 leads to increased mitochondrial fission mediated by upregulation of dynamin related protein 1 (Drp1), resulting in abnormal mitochondrial functions. CEND1 deficiency leads to cognitive impairments in mice. Overexpression of CEND1 in the hippocampus of 5xFAD mice rescued cognitive deficits. Moreover, we identified that CDK5/p25 interacted with and phosphorylated CEND1 which promoted its degradation. Our study provides new mechanistic insights in mitochondrial function regulations by CEND1 in Alzheimer's disease.

Cell Death & Differentiation (2022) 29:2417–2428; <https://doi.org/10.1038/s41418-022-01027-7>

INTRODUCTION

Brain is one of the highly metabolic organs, and neurons of the central nervous system have a strong demand for mitochondria [1]. Extensive damage to mitochondria leads to cell death because they can no longer produce enough energy [2]. Mitochondria are highly dynamic organelles playing an important role in neuron survival by participating in fusion and fission events, ATP production [3], calcium homeostasis [4], cell death [5], reactive oxygen species (ROS) production [6], and metabolism [7]. Multiple lines of evidence suggest that mitochondrial dysfunction is involved in AD pathogenesis, but the mechanism is not fully understood. Mitochondrial dysfunction occurs in the early stage of AD [8], including diminished glucose metabolism, increased ROS production, disruption of the balance between mitochondrial fusion and fission, decreased axonal transport of mitochondria, and changed mitochondrial morphology [9, 10].

Morphological mitochondria changes are regulated by a series of fusion and fission proteins. The fusion proteins include dynamic GTPase regulator optic atrophy 1 (OPA1), Mitofusin 1 (MFN1), and Mitofusin 2 (MFN2). The fission proteins are composed of dynamin-like GTPase regulator dynamin related protein 1 (Drp1) and mitochondrial fission 1 protein (Fis1). Drp1 is one major protein involved in the division of mitochondria, whose activity is regulated by post-translational modifications such as phosphorylation, S-nitrosylation, SUMOylation, and O-GlcNAcylation [11–16]. Phosphorylation of Drp1 at S616 can increase its capability to promote mitochondrial fission [17, 18]. MARCH-V, a mitochondrial

E3 ubiquitin ligase, ubiquitinates Drp1 and regulates Drp1-mediated mitochondrial fission [19].

Cell cycle exit and neuronal differentiation 1 (CEND1, also known as BM88; gene for *Cend1*) is a 22 kDa organelle membrane inserted protein [20, 21]. CEND1 anchors to intracellular membranes via a transmembrane domain of 20 hydrophobic amino acids, followed by a short tail of three positively charged residues (RKK) on the C-terminus. CEND1 exclusively expresses in the nerve system and plays important roles in neuronal differentiation [22]. Overexpression of CEND1 in neural progenitor cells or neuroblastoma cells inhibits cell cycle and promotes neuronal differentiation by downregulating cell cycle proteins [23] and increasing neuronal markers (β -tubulin and synaptophysin) [22, 24, 25] respectively. Previous data reported that *Cend1* knockout mice display impaired cerebellar development [26]. However, the exact function of CEND1 has not yet been fully uncovered, especially in AD.

Cell cycle regulation also participates in regulation of mitochondrial fusion/fission and energy production [27, 28]. Cyclin dependent kinases (CDKs) are central cell cycle regulatory enzymes. Among them, CDK5 is a unique CDKs family member which is activated by non-cyclin protein p35. During pathogenesis of AD, p35 is cleaved by calpain to generate a more stable fragment p25, which induces overactivation of CDK5 [29, 30]. The exorbitant activation of CDK5 can promote mitochondrial fission and damage mitochondrial activity [31–34]. Pharmacological inhibition or genetic knockdown of CDK5 could attenuate amyloid- β (A β)-induced mitochondrial fission [34].

¹Institute of Neuroscience, College of Medicine, Xiamen University, Xiamen, Fujian 361005, China. ²Fujian Key Laboratory of Molecular Neurology, Institute of Neuroscience, Fujian Medical University, Fuzhou, Fujian 350004, China. ³Department of Anesthesiology, The First Affiliated Hospital of Xiamen University, Xiamen, Fujian 361005, China. ⁴These authors contributed equally: Wenting Xie, Dong Guo, Jieyin Li. ✉email: gaoww@fjmu.edu.cn; jiezhang@xmu.edu.cn
Edited by N. Bazan

Received: 18 November 2021 Revised: 1 June 2022 Accepted: 4 June 2022
Published online: 22 June 2022

Here, we found that CEND1 was exclusively a neuronal mitochondrial protein and decreased significantly in the brain of AD mice. Depletion of CEND1 in primary neurons and mice induced mitochondrial fission dysfunctions by upregulation of Drp1. CEND1 knockout mice exhibited learning and memory impairments. Moreover, overexpression of CEND1 in hippocampus of 5xFAD mice restored mitochondrial function and improved memory and learning ability. Finally, we identified that CDK5/p25 bound to and phosphorylated CEND1 at serine 10, promoting CEND1 degradation. Taken together, these results demonstrated that the CDK5-CEND1-Drp1 axis plays important roles in mitochondrial function regulation and pathogenesis of AD.

MATERIALS AND METHODS

Reagents

Anti-CEND1, COX IV, p-Drp1 (ser616), MAP2, PSD95, GluR1, Synapsin, Synaptophysin and cleaved caspase3 antibodies were from CST. Anti-p35 (c-19), CDK5 (c-8) and GFP antibodies were from Santa Cruz. Anti-Tuj1, NeuN, HA and Thiophosphate easter antibodies were from Abcam. An anti-GFP (FL) antibody, Acetyl-CoA, DTNB, oxaloacetate and DAPI were from Sigma-Aldrich. Anti-Drp1, OPA1, HA, MFN2, β -actin, GAPDH, α -tubulin and GST antibodies were from Proteintech. APP and β -actin antibodies were from Life Technologies. Fluorescent secondary antibodies, HRP-conjugated secondary antibodies and MitoTracker Red were from ThermoFisher Scientific. MK8931, CQ, MG132 and Mdivi-1 were from MCE. Cell culture reagents were from Gibco. Reagents for plasmid construction were from Takara Bio Inc.

Animals and generation of CEND1 knockout mice

All mice were kept and bred at Xiamen University Laboratory Animal Center and all experiments were carried out in accordance with protocols by the Institutional Animal Care and Use Committee at Xiamen University. The *Cend1*^{-/-} mice were generated from Beijing Biocytogen Co., Ltd. The 5xFAD and APP/PS1 mice were purchased from Model Animal Research Center of Nanjing. Six-month-old and littermate mice were used for behavioral tests. *Cdk5*^{+/-} mice was maintained on a mixed C57BL/6J background. Wild type C57BL/6J mice were purchased by Xiamen University Laboratory Animal Center.

Transmission electron microscope and immunoelectron microscopy

The animal tissues were collected rapidly and 2.5% glutaraldehyde fixation solution (immunoelectron microscopy 0.5% glutaraldehyde fixation) should be put into the tissue within the shortest time (within 1 min) after the tissue was removed from the living body. Then the tissues were handled by Core Facility of Biomedical Sciences, Xiamen University. Images were taken by Hitachi HT-7800.

Mitochondrial oxygen consumption

Primary neurons were seeded in XF 96 Cell Culture Microplates (Seahorse, Agilent Technologies) at a concentration of 50,000 cells/well. On the 7th day, the primary neurons were infected with virus. The culture medium was removed from each well and replaced by Seahorse Xfe Base Medium pre-warmed at 37 °C and supplemented with B27 and 1 mM glutamine, pH 7.4 (± 0.4). Cells were incubated in a CO₂-free incubator at 37 °C for 1 h. Oligomycin, phenylhydrazine (FCCP), rotenone and antimycin A were added in different times. Oxygen consumption rate (OCR) values were acquired.

Data independent acquisition (DIA) and mass spectrum

Fresh brain Cortex /hippocampus samples were obtained from three 7-month-old 5xFAD mice and three litters of control mice. Then mitochondria were isolated from brain tissue. Mitochondrial protein quantitative analyses were performed with Bruker TimsTOF Pro for a data independent acquisition mass spectroscopy. The mass spectrometry proteomics data have been deposited to the ProteomeXchange Consortium (<http://proteomecentral.proteomexchange.org>) via the iProX partner repository with the dataset identifier PXD032992.

Cortex/hippocampus lysates of 6-month-old *Cend1*^{+/+} and litter of *Cend1*^{-/-} mice were obtained the same way as above, and then were

mixed with anti-CEND1 or IgG antibodies. Acquired proteins were subjected to SDS-PAGE electrophoresis. After Coomassie brilliant blue staining, the gel was cut into 1.5 mm \times 1.5 mm blocks and subjected to Bruker TimsTOF Pro analysis.

Mitochondria isolation and trypsin digestion

After washing, cells were pelleted by centrifugation at 500 g for 5 min. Cells were then suspended in Mito-Lysis buffer (0.25 M sucrose, 1 mM EDTA, adjusted to pH 7.6) and homogenized on ice with a homogenizer. The homogenate was centrifuged at 1500 g for 10 min, and the supernatant was collected and then centrifuged at 14,000 g for 10 min. The supernatant was collected as the cytosol fraction, while the pellet was suspended with Mito-Lysis buffer and collected as the mitochondria fraction. Intact mitochondria were mixed with indicated concentration of trypsin in Mito-Lysis buffer and incubated at 30 °C for 2 h.

Citrate synthase activity assay

50 μ g of cell lysate was added to 160 μ l of assay buffer (60 mM Tris-HCl, Ph7.5, 200 mM Acetyl-CoA, and 250 mM DTNB) and incubated for 5 min. 20 μ l of 2 mM oxaloacetate was added. OD was measured at 412 nm for 20 min using a spectrometry plate reader. The rate of citrate synthase activity was quantified relative to control cells.

In vitro kinase assay

Recombined protein purified from *E. coli* was incubated with CDK5/p25 kinase and ATP- γ -S (final concentration 10 mM) in 1x kinase assay buffer (25 mM Tris-HCl (pH 7.5), 5 mM beta-glycerophosphate, 2 mM dithiothreitol (DTT), 0.1 mM Na₃VO₄ and 10 mM MgCl₂) at 30 °C for 45 min. PNBM (final concentration 10 μ M) was added into the mixture and incubated at room temperature for 1 h. Samples were subjected to Western blotting and phosphorylated proteins were immunoblotted by an anti-Thiophosphate ester antibody.

Western blotting

Cultured cells and mouse brain tissues were homogenized in lysis buffer (RIPA) on ice for 40 min, and subsequently centrifuged at 12,000 rpm for 10 min at 4 °C. Supernatants were separated on 8–15% SDS-PAGE gels and transferred to Immobilon-P PVDF membrane (Millipore). Primary antibodies were incubated overnight at 4 °C after blocking with 5% non-fat milk. The membrane was washed three times and then incubated with secondary HRP-conjugated antibodies for 1 h at room temperature. Finally, the blots were washed and immune-detected proteins were visualized using ECL method. Full-length original western blots for the results are provided in Supplementary materials.

Stereotactic injection of adeno-associated virus

AAV2/9-syn-GFP-P2A-*Cend1*-3FLAG and AAV2/9-syn-GFP-P2A-U6-sh *Cend1* viruses were purchased from OBio Biotech Shanghai. Viruses were stereotactically injected into the hippocampus. Two months after injection, mice were sacrificed after behavior tests, then brains were harvested for histological immunofluorescence staining and western blotting.

Animal behavioral tests

Morris water maze test. It is mainly used to test the learning and memory ability of spatial position and orientation (spatial orientation) in experimental animals. In this study, the water maze used a 120 cm circular tank in diameter with a platform in SW quadrant filled with water (22 \pm 2 °C). The walls of the tank were posted four different shapes served as reference cues. The training continued for 4–6 consecutive days until the mice found target platform within 1 min and maintained 10 s in the platform. Mice were randomly started at each of four points (N, S, E, W) in daily training. On test day, the platform was removed, mice were placed in the NE point swimming for 1 min. First latency to target, the number of target (platform) crossings and the time spent in every of the four quadrants were recorded.

Fear conditioning test

The fear conditioning test is used to study the environmental conditioned fear of small rodents. Contextual test is related to memory in the hippocampus and Cue test is related to fear memory in the amygdala. This test consists of three stages: The first day were training stage, mice stimulated by vocal, light and shock; On the second day, mice were placed

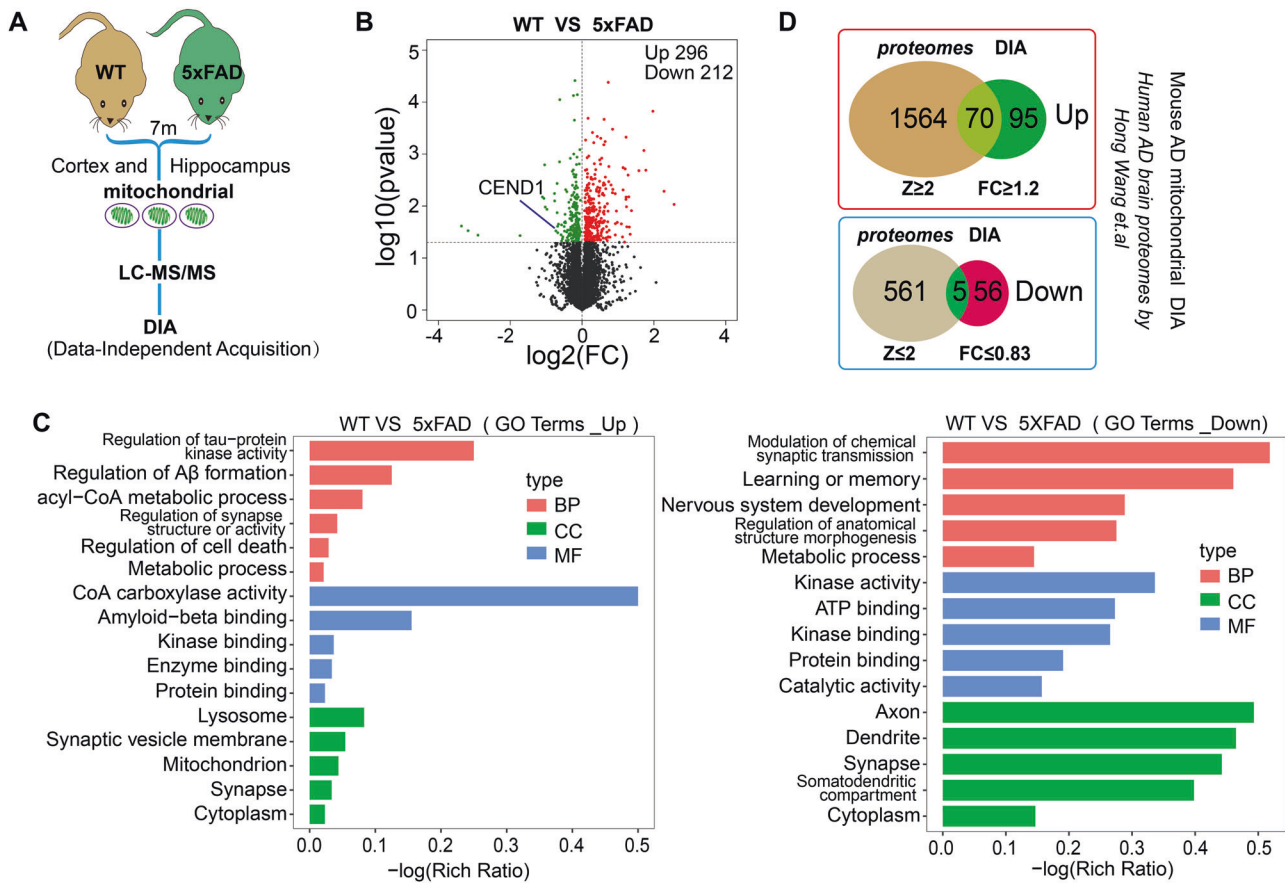


Fig. 1 Data independent acquisition (DIA) analysis for AD mitochondrial proteome. **A** Schematic diagram of the experimental flow of DIA experiment. **B, C** A total of 508 differentially expressed mitochondrial proteins in 5xFAD mice brain were clustered using Volcano plot (**B**) and GO (**C**) parameters. **D** The overlap between AD mitochondrial proteome database with AD patient's database.

in the test chamber without any stimulation for 5 min to assess context-associated fear conditioning (contextual test); On the third, mice were placed in the test chamber without any stimulation for 3 min and then 3 min vocal stimulation to assess amygdala-associated fear conditioning (cued test).

T/Y maze test

T/Y mazes are used to evaluate spatial alternation and working memory. Every test mouse was placed in the middle of maze, then freely moving 5 min. Alternation Triplet % were used to define consecutive triplets of different arm choices.

Rotarod test

Mice were placed on an accelerated rotarod. The instrument was then accelerated to 60 rpm/min, and the latency to fall (in seconds) was recorded. Before test mice were trained to learn to run. Four consecutive trials were repeated, which averaged latency to fall was analyzed.

Statistical analysis

Statistical analysis was performed with Prism 8 (GraphPad Software Inc.) and quantification results were showed as mean \pm SEM. Statistical significance was determined using unpaired Student's *t* test or analysis of variance (ANOVA) test. Significance values are indicated by asterisks: *, $p < 0.05$; **, $p < 0.01$; ***, $P < 0.001$.

RESULTS

Data independent acquisition (DIA) analysis for AD mitochondrial proteome

Abnormal mitochondrial dynamics in nerve cells participates in the pathogenesis of AD, but the detailed mechanism is unclear.

We applied the DIA-based mass spectrometry quantification strategy to evaluate the mitochondrial proteome changes in brain of 5xFAD and control mice (Fig. 1A). From comprehensively integrated analyses of the enriched peptides, 296 upregulated and 212 downregulated proteins in 5xFAD vs WT mice were found (Fig. 1B). Gene ontology (GO) enrichment analysis of biological process from quantifiable proteins is summarized (Fig. 1C), which highlights the upregulated enriched terms such as regulation of A β formation, regulation of tau-protein kinase activity, amyloid-beta binding; downregulated terms put more emphasis on modulation of chemical synaptic transmission, learning and memory.

Next, we compared our AD mice mitochondrial DIA data with the published proteomic dataset of human AD patients [35]. Notably, seventy-five common proteins were found (Fig. 1D). Among the overlapped downregulated proteins, CEND1 draws our attention. The downregulation of CEND1 in AD patients and mouse brain suggested that the potential roles of CEND1 in the pathogenesis of AD.

CEND1 is a neuron-specific mitochondrial protein

We collected different tissues from mouse and detected the expression pattern of CEND1. CEND1 is exclusively expressed in the nerve system such as cortex, cerebellum and hippocampus (Fig. 2A). Moreover, CEND1 increases significantly in hippocampus during development, GluR1 and SNAP25 serve as positive controls (Fig. 2B). By comparing CEND1 expressions in cultured neurons, microglia, and astrocytes, we found that CEND1 expresses predominantly in neuron (Fig. 2C).

Further subcellular fractions analysis and immunofluorescent staining both revealed that CEND1 mostly locates in mitochondria

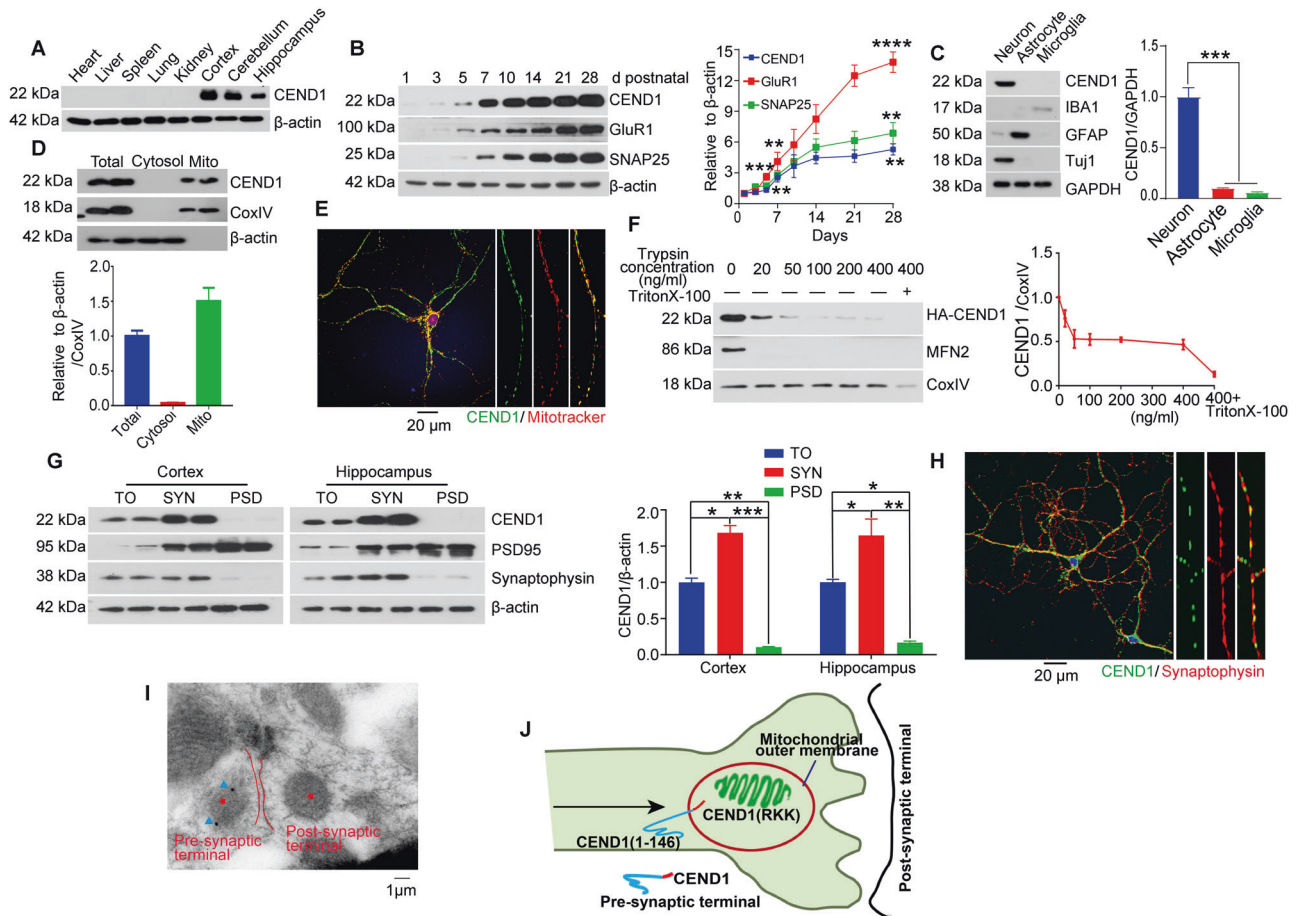


Fig. 2 CEND1 is a neuron-specific mitochondrial protein. **A** Expression levels of CEND1 protein in different tissues of adult C57BL/6 mouse. Tissue samples were subjected to Western blotting for CEND1 with β -actin as a loading control. **B** Developmental expression of CEND1 protein in the hippocampus of C57BL/6 mouse. GluR1 and SNAP25 are markers of mature neurons. Statistical analyzed the protein levels of CEND1, SNAP25 and GluR1 in P1, P7 and P28 samples. mean \pm SEM, $n = 3$ per sample, $**p < 0.01$, $***p < 0.001$ by two-tailed Student's t -test. **C** Expression levels of CEND1 protein in mature primary cortical neurons, astrocytes and microglia cultured in vitro. mean \pm SEM, $n = 3$ per group, $***p < 0.001$, by ANOVA with Dunnett's test for post-hoc analysis. **D** 2-month-old C57BL/6 mouse were separated into the cytosolic fraction and mitochondrial fraction, after which samples were subjected to Western blotting for CEND1 and β -actin serves as a cytosolic marker and COXIV as a mitochondrial marker, $n = 3$ per group. **E** Mature primary cortical neurons at DIV13 were stained with mitochondrial dye, MitoTracker. Co-localization of CEND1 and MitoTracker was shown. Scale bar, 20 μ m. **F** Intact mitochondria isolated from HEK 293 T cells transfected with HA-CEND1 were digested with indicated concentrations of trypsin for 2 h. Mitochondria treated with TritonX-100 and 400 ng/ml trypsin were considered as the negative control. MFN2 is the marker protein of mitochondrial outer membrane and COX IV is an inner membrane marker protein. $n = 3$ per group. **G** Western blotting showing enrichments of CEND1 in synaptic fractions enriched from 2-month-old C57BL/6 mouse cortex and hippocampus. mean \pm SEM, $n = 4$ per sample, $**p < 0.01$, $***p < 0.001$ by ANOVA with Dunnett's test for post-hoc analysis. **H** Mature primary cortical neurons at DIV13 were stained with CEND1 and pre-synapse marker synaptophysin. Scale bar, 20 μ m. **I** Immunoelectron microscopy analysis of 2-month-old C57BL/6 mouse hippocampus stained with CEND1 antibody. Scale bar, 1 μ m. **J** Schematic diagram of the location of CEND1.

(Fig. 2D, E). Upon trypsin digestion of intact mitochondria, proteins associated with the outer membrane of mitochondria was digested (like MFN2), while proteins associated with the inner membrane remain stable (like COX IV, which could be digested only after disruption of the outer membrane by Triton X-100). We found that CEND1 could be digested by trypsin without treatment with Triton X-100 (Fig. 2F), indicating that CEND1 locates in the outer membrane of mitochondria. We next identified that the last three amino acids residues (147-149, RKK) at C-terminal of CEND1 mediate its outer membrane mitochondrial localization, since CEND1 protein with RKK deletion or RKK to AAA mutation does not locate in mitochondria (Fig. S1). By pre-/post synapses isolation, immunofluorescent staining and immunoelectron microscopy analysis, we further revealed that CEND1 enriches in pre-synapse fraction (Fig. 2G-I).

Together, these results showed that CEND1 is a neuronal specific protein which locates in outer membrane of mitochondria and pre-synapse (Fig. 2J).

CEND1 is reduced in AD cell and mouse models

To further investigate the expression of CEND1 during the pathogenesis of AD, hippocampus from different aged AD mice (APP/PS1 and 5xFAD) were collected. We found that CEND1 protein levels were significantly decreased in hippocampus of 10-month old APP/PS1 mice compared with the age-matched wild type mice (Fig. 3A). By analysis of 2-, 4-, 6- and 9-month-old 5xFAD mice and their age-matched controls, we found that CEND1 decreased significantly with the progression of AD (Fig. 3B, C). The similar results were also found in AD cell models. A β (1-42) treatments in primary neurons or APP overexpression in N2a cells (N2a-APP695 [36]) both decreased CEND1 expression dramatically (Fig. 3D, E). The mRNA level of *Cend1* was not found difference in brain of 5xFAD mice compared with wild type mice (Fig. 3F). MK8931, a BACE1 inhibitor, effectively alleviated the decrease of CEND1 in primary neurons derived from 5xFAD mice (Fig. 3G).

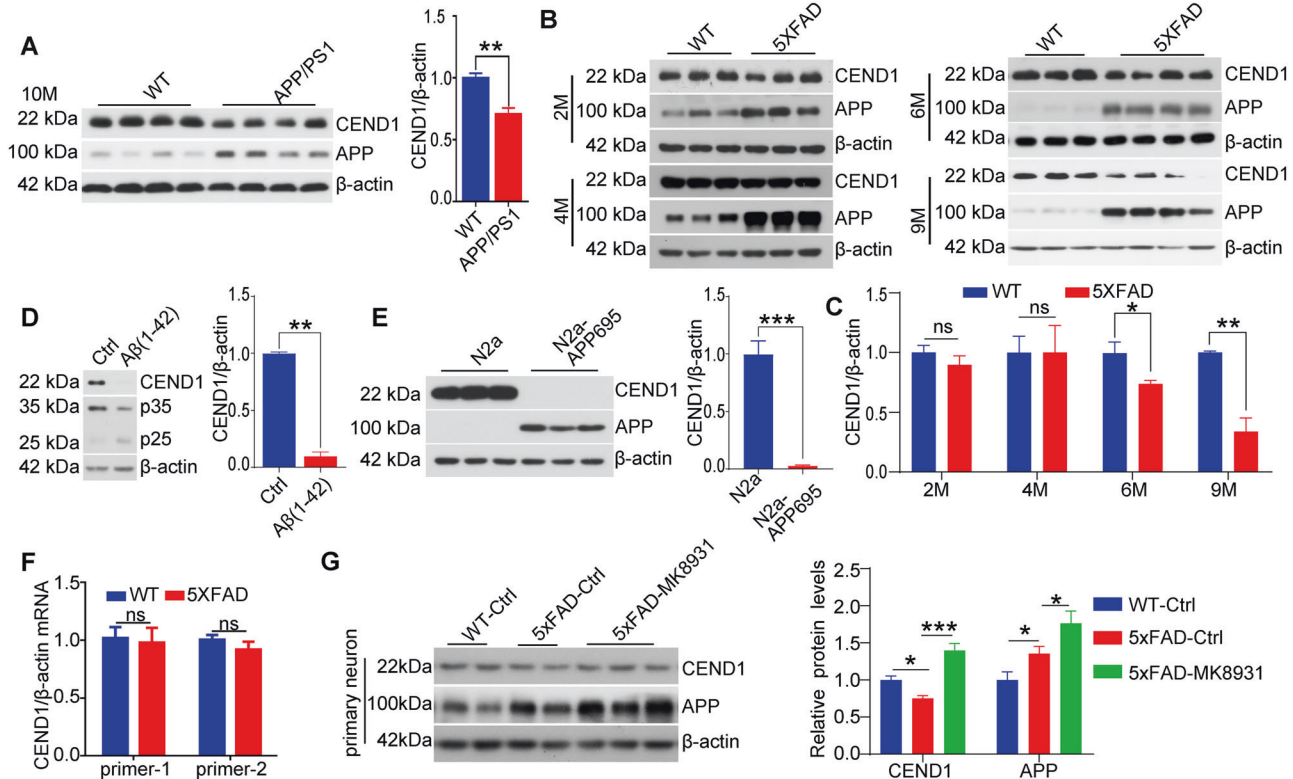


Fig. 3 Downregulation of CEND1 in AD mice brain and cell lines. **A** Hippocampus of APP/PS1 mice at the age of 10-month-old and age-matched controls were subjected to Western blotting analysis for CEND1, APP with β -actin as the loading control. mean \pm SEM, $n = 4$ per sample, $**p < 0.01$, by two-tailed Student's t -test. **B, C** Hippocampus lysates of 5xFAD mice at the age of 2, 4, 6, 9 month and age-matched controls were subjected to western blotting analysis for CEND1, APP with β -actin as control. mean \pm SEM, $n \geq 4$ per group, $*p < 0.05$, $**p < 0.01$, by two-tailed Student's t -test. **D** Mature primary cortical neurons were treated with $10 \mu\text{M}$ $\text{A}\beta(1-42)$ for 24 h. Protein lysates were subjected to Western blotting for CEND1, p35 and p25. mean \pm SEM, $n = 3$ per group, $**p < 0.01$, by two-tailed Student's t -test. **E** N2a and N2a-APP695 cells were subjected to western blotting analysis for CEND1 and APP. β -actin was used as the internal control. mean \pm SEM, $n = 3$ per group, $***p < 0.001$, by two-tailed Student's t -test. **F** RT-PCR analysis of 9-month-old 5xFAD mice hippocampus for CEND1. mean \pm SEM, $n = 3$ per group, $*p < 0.05$, by two-tailed Student's t -test. **G** 5xFAD and control primary cortical neurons were treated with 8 nM MK8931 for 12 h. Protein lysates were subjected to Western blotting for CEND1, APP and β -actin. mean \pm SEM, $n = 3$ per group, $*p < 0.001$, $***p < 0.001$, by ANOVA with Dunnett's test for post-hoc analysis.

CEND1 is crucial for learning and memory function

To assess the roles of CEND1 in AD pathogenesis, we first generated the CEND1 knockout mice ($Cend1^{-/-}$) (Fig. S2A). CEND1 deletion in $Cend1^{-/-}$ mice was confirmed by RT-PCR (Fig. S2B), Western blotting and immunostaining (Fig. 4A, B). CEND1 deletion had no effects on the body weight, brain weight or the lifespans (Fig. S2C–F). As mentioned above, CEND1 specifically expresses in neurons, we assessed potential cognitive deficits in $Cend1^{-/-}$ mice using behavioral tests. In Morris water maze tests, we found that $Cend1^{-/-}$ mice showed impaired learning with increased escape latency compared with controls ($Cend1^{+/+}$) during the 5-days training phase (Fig. 4C). Moreover, during the probe trial test, in which the hidden platform was removed on day 6, $Cend1^{-/-}$ mice spent significantly less time in the target quadrant and demonstrated fewer entries into the platform location and required a longer period to travel from the entry point to the target zone compared with controls (Fig. 4D–F). In T-maze test, $Cend1^{-/-}$ mice showed less crossing time in three continuous arms compared to controls (Fig. 4G, H). We performed rotarod assay to test for locomotor activity and found no differences between $Cend1^{-/-}$ and control mice (Fig. 4I).

To approve that the above phenomena we observed were not caused by the abnormal neuronal development, we depleted the expression of CEND1 in adult WT mice through shRNA-AAV injection. U6 promoter-driven $Cend1$ shRNA expression system was established in AAV2/9 vector, with GFP expression controlled

by a SYN promoter (pAAV-SYN-eGFP-U6-sh*Cend1* short for AAV-eGFP-sh*Cend1*). As shown in Fig. 4J, AAV-eGFP-sh*Cend1* or a control (AAV-eGFP-shRNA) were injected into hippocampus of 2-month-old WT mice. The CEND1 knockdown efficiency was confirmed by western blotting (Fig. 4K). The Morris water maze tests were performed 1.5 months after injection. As shown in Fig. 4L–O, CEND1 knockdown also significantly impaired the mouse learning and memory. Furthermore, CEND1 deficiency or knockdown decreased the neuronal dendritic branching and synaptic proteins levels (Fig. S3A–D), and induced neuronal apoptosis (Fig. S4A–C) in primary cultured neuron.

CEND1 deficiency accelerates learning and memory impairments in 5xFAD mice

To assess the role of CEND1 in AD, we crossed $Cend1$ heterozygous knockout ($Cend1^{+/-}$) mice with 5xFAD& $Cend1^{+/-}$ mice to generate four groups of mice ($Cend1^{+/+}$ (WT), $Cend1^{-/-}$, 5xFAD, and 5xFAD& $Cend1^{-/-}$ mice) (Fig. 5A). The CEND1 deletion efficiency in 5xFAD& $Cend1^{-/-}$ mice was confirmed by western blotting (Fig. 5B). The APP expression and amyloid plaque burden were not affected (Fig. 5B, C), but the neuronal death was significantly increased in the hippocampus of 5xFAD& $Cend1^{-/-}$ mice compared to 5xFAD mice (Fig. 5D). We next performed cognitive behavioral tests in these mice. Rotarod assay was used for locomotor activity test and found no differences (Fig. 5E). In Morris water maze test, 5xFAD& $Cend1^{-/-}$ mice

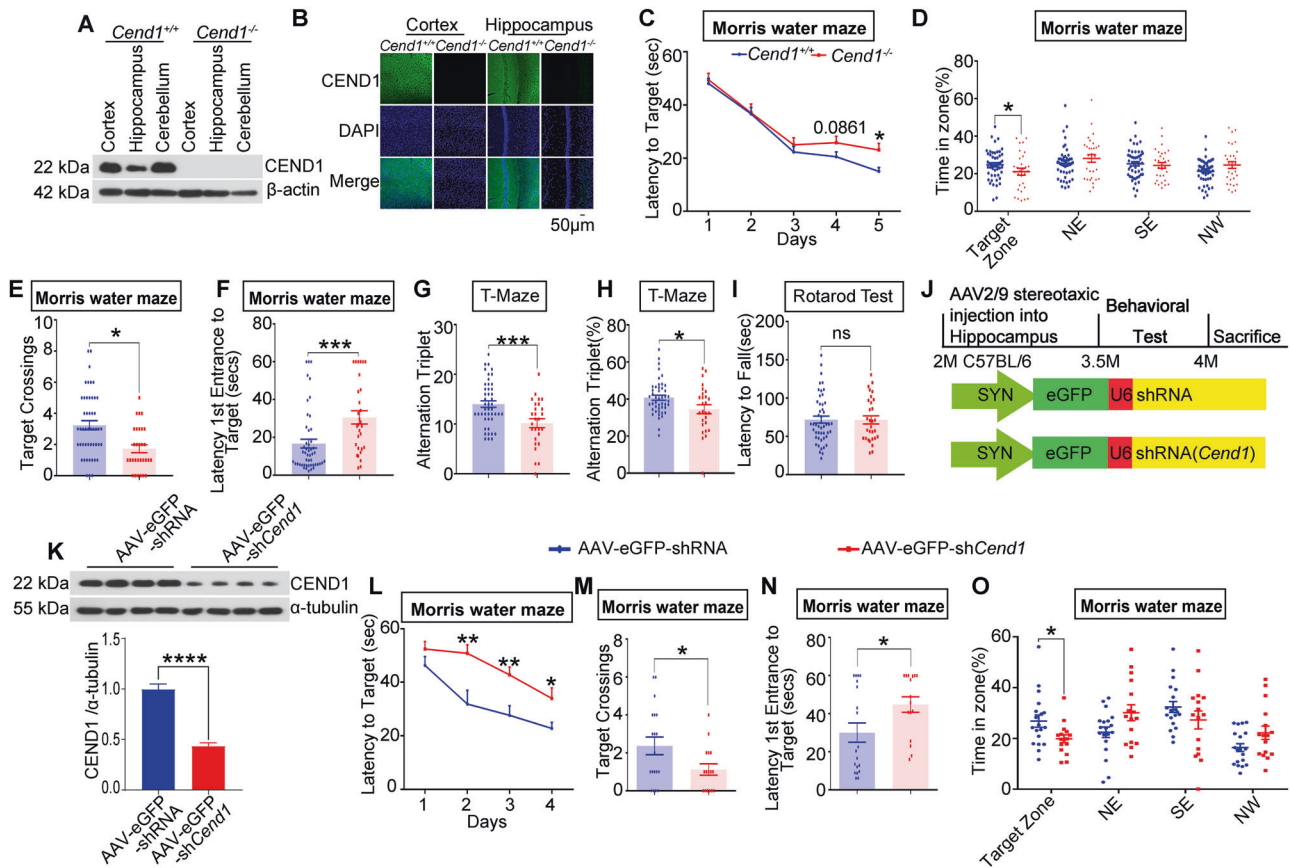


Fig. 4 CEND1 knockout and knockdown impaired learning and memory functions. **A** Representative western blotting of CEND1 protein levels in the cortex, hippocampus and cerebellum from *Cend1*^{+/+} and *Cend1*^{-/-} mice. β -actin was used as the internal control. **B** Representative confocal images showing CEND1 expression via immunofluorescent staining in *Cend1*^{+/+} and *Cend1*^{-/-} mice. Scale bar, 50 μ m. **C** MWM analysis as latency to target in the invisible platform trainings. **D–F** MWM analysis as time in zone (%) in the invisible platform tests, target cross number and latency 1st entrance to target (secs) in 6-month-old *Cend1*^{+/+} ($n = 49$ mice), *Cend1*^{-/-} ($n = 30$ mice). **G, H** 6-month-old *Cend1*^{+/+} and *Cend1*^{-/-} mice were analyzed for alternation triplet by T-maze tests. *Cend1*^{+/+} ($n = 46$ mice), *Cend1*^{-/-} ($n = 27$ mice). **I** *Cend1*^{+/+} and *Cend1*^{-/-} mice behavior in rotarod test in 6-month-old *Cend1*^{+/+} ($n = 49$) and *Cend1*^{-/-} ($n = 30$) mice. **J** Schematic for the generation of CEND1 knockdown mice, behavioral tests, and expression analysis. **K** CEND1 protein levels in mouse brain injected with AAV-eGFP-shCend1 or control AAV-eGFP-shRNA were determined by western blotting, α -tubulin was used as the internal control. **L** Initial latency time to target was recorded during the four days training course. **M–O** MWM analysis as target cross number, latency 1st entrance to target (secs), time in zone (%) in the invisible platform tests in control AAV-eGFP-shRNA ($n = 19$) and AAV-eGFP-shCend1 ($n = 16$) mice. mean \pm SEM, * $p < 0.05$, ** $p < 0.01$, by two-tailed Student's *t*-test.

exhibited worsening learning and memory than 5xFAD mice (Fig. 5F–I). We next evaluated contextual and cued learning response in these mice using fear conditioning tests. Freezing response was found to be significantly reduced in response to contextual testing and cued testing in 5xFAD&*Cend1*^{-/-} mice compared with 5xFAD mice (Fig. 5J, K). Taken together, these results demonstrate that CEND1 deficiency exacerbates cognitive impairments in AD mice.

Overexpression of CEND1 rescues cognitive impairments and synaptic deficits in 5xFAD mice

To test whether CEND1 expression could rescue impaired learning and memory defects in AD mice, we generated an AAV construct in which CEND1 is expressed using a SYN promoter (AAV-SYN-GFP-P2A-Cend1, short for AAV-GFP-CEND1) (Fig. 6A). AAV-GFP-CEND1 or AAV-GFP control were injected into the hippocampus of 4.5-month-old 5xFAD mice (Fig. 6A), and the overexpression of CEND1 was confirmed by western blotting and immunostaining (Fig. 6B, C). Next, we found that CEND1 ectopic expression rescued cognition impairments in Morris water maze test (Fig. 6D, E), T-maze test (Fig. 6F, G) and fear conditioning contextual test (Fig. 6H) without affecting the locomotor activity in AD mice (Fig. 6I).

CEND1 modulates mitochondrial dynamic by regulating Drp1

Considering the specific mitochondrial localization, we next investigate the effect of CEND1 on mitochondrial function. We first found that CEND1 deficiency increased the mitochondrial number and reduced the mitochondrial area and diameter measured by electron microscopy analysis (Fig. 7A). The mitochondrial mass was also significantly damaged in CEND1 knockout neurons (Fig. 7B). To determine the mechanism underlying CEND1-affected mitochondrial morphology, we analyzed CEND1-associated proteins in mouse brain by immunoprecipitation in combination with mass spectrometry (IP-MS). We identified eighteen CEND1 interaction proteins which locate in mitochondria, including five mitochondrial dynamics proteins, three OXPHOS proteins, two permeability transition pore proteins and eight metabolism proteins (Fig. S5A, B).

Given the mitochondrial morphology defects, we examined levels of the mitochondrial fission protein Drp1 and Drp1 (S616), as well as mitochondrial fusion protein MFN2 and OPA1 in vivo and in vitro. Notably, Drp1 and Drp1 (S616) were both increased and MFN2 was reduced in CEND1-deficient hippocampus or primary neurons compared with their controls (Fig. 7C, Fig. S5C, D). In contrast, overexpression of CEND1 in hippocampus of 5xFAD by AAV-CEND1 injection or in N2a-APP695 cells by CEND1 overexpression only

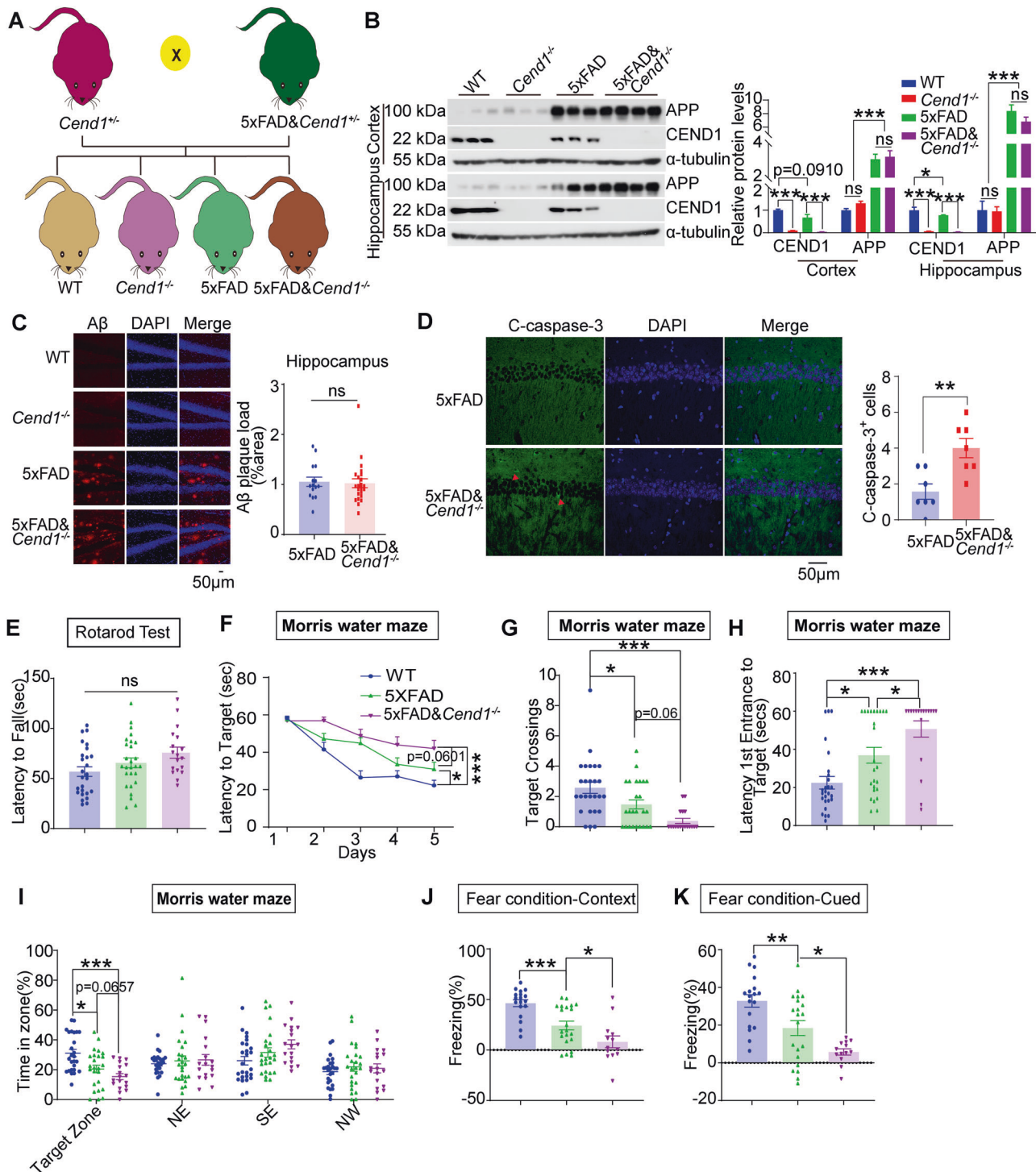


Fig. 5 CEND1 deficiency accelerates learning and memory impairment in 5xFAD Mice. **A** Schematic illustration of *Cend1*^{-/-} mice cross with 5xFAD mice. **B** Protein levels of CEND1 in the cortex and hippocampus of 7-month-old WT ($n = 3$), *Cend1*^{-/-} ($n = 3$), 5xFAD ($n = 3$), and 5xFAD&*Cend1*^{-/-} ($n = 3$) mice; α -tubulin was used as the internal control; Overexpression of APP indicates the 5xFAD mice. mean \pm SEM, * $p < 0.001$, *** $p < 0.001$, by ANOVA with Dunnett's test for post-hoc analysis. **C** Representative confocal images showing A β expression in the hippocampus via immunofluorescent staining compared of 7-month-old WT ($n = 4$), 5xFAD ($n = 4$), and 5xFAD&*Cend1*^{-/-} ($n = 4$) mice. mean \pm SEM, * $p < 0.05$, by two-tailed Student's t -test. Scale bar: 50 μ m. **D** Immunofluorescence staining for cleaved caspase-3 as an apoptotic marker in the 5xFAD&*Cend1*^{-/-} ($n = 3$) mice as compared to 5xFAD littermates ($n = 3$). The red triangle represents the positive cells. mean \pm SEM, ** $p < 0.01$, by two-tailed Student's t -test. Scale bar: 50 μ m. **E** Rotarod tests of 7-month-old WT ($n = 26$), 5xFAD ($n = 27$) and 5xFAD&*Cend1*^{-/-} ($n = 18$) mice. **F** MWM analysis as latency to target in the invisible platform trainings. **G–I** MWM analysis as target cross number, latency 1st entrance to target (secs), time in zone (%) in the invisible platform tests in 7-month-old WT ($n = 26$), 5xFAD ($n = 25$), and 5xFAD&*Cend1*^{-/-} ($n = 18$) mice. **J, K** In fear conditioning tests, WT ($n = 18$), 5xFAD ($n = 21$), and 5xFAD&*Cend1*^{-/-} ($n = 13$) mice were initially subjected to training and their freezing response with contextual and cued fear stimuli was measured as a percentage of the testing duration. mean \pm SEM, * $p < 0.001$, ** $p < 0.001$, *** $p < 0.001$, by ANOVA with Dunnett's test for post-hoc analysis.

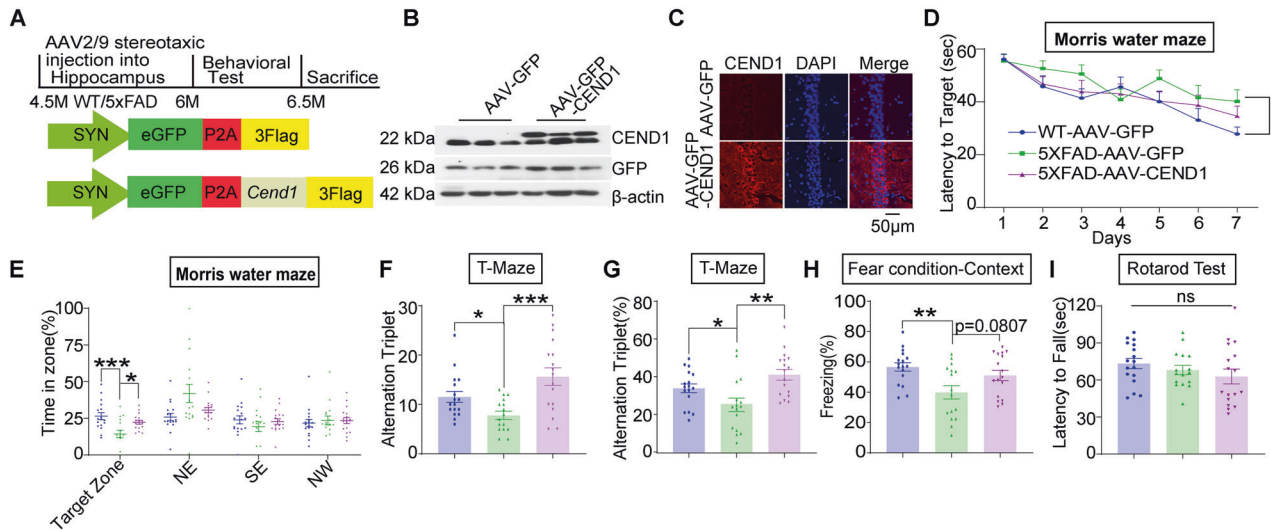


Fig. 6 CEND1 overexpression rescues cognitive impairment and synaptic deficits in 5xFAD mice. **A** Workflow diagram for AAV-GFP-CEND1 injection and subsequent analysis. **B** Hippocampal lysates from 5xFAD mice injected with AAV-GFP-CEND1 or controls (AAV-GFP) were subjected to Western blotting for CEND1, GFP, and β -actin (AAV-GFP-CEND1, $n = 3$; AAV-GFP, $n = 3$). **C** Representative CEND1 fluorescence images of hippocampus after AAV injection. Scale bar, 50 μ m. **D**, **E** In the Morris water maze test, AAV-GFP WT ($n = 17$), AAV-GFP 5xFAD ($n = 16$) and AAV-GFP-CEND1 5xFAD ($n = 17$) mice were evaluated for escape latency over a 7-day training. On the 8th day, percentage of time the mice spent in the target zone were quantified. **F**, **G** Alternation triplet by T-maze tests in 6.5-month-old AAV-GFP WT ($n = 17$), AAV-GFP 5xFAD ($n = 16$) and AAV-GFP-CEND1 5xFAD ($n = 17$) mice. **H** In the fear conditioning test, freezing percentage was assessed to evaluate contextual memory 24 h after training. Representative traces are shown. AAV-GFP WT mice ($n = 17$), AAV-GFP 5xFAD mice ($n = 16$) and AAV-GFP-CEND1 5xFAD mice ($n = 17$). **I** Rotarod test of 6.5-month-old AAV-GFP WT ($n = 17$), AAV-GFP 5xFAD ($n = 16$) and AAV-GFP-CEND1 5xFAD ($n = 17$) mice. mean \pm SEM, * $p < 0.001$, ** $p < 0.001$, *** $p < 0.001$, by ANOVA with Dunnett's test for post-hoc analysis.

resulted in reduced Drp1 level without affecting OPA1 (Fig. 7D, Fig. S5E, F). These data suggested that Drp1 may be the important target of CEND1. Meanwhile, overexpression of GFP-CEND1 in SH-SY5Y cells increased mitochondrial length (Fig. S5G). Next, we explored the mechanism underlying the regulation of Drp1 by CEND1 and found that CEND1 associates with Drp1 (Fig. 7E). Cycloheximide (CHX) treatment assay showed that CEND1 overexpression significantly accelerates the degradation of Drp1 in HEK-293 T cells (Fig. 7F). To determine the degradation pathway of Drp1 induced by CEND1, ubiquitin-proteasome inhibitor MG-132 or autophagy inhibitor Chloroquine (CQ) were treated the cells after CHX administration. We found that the downregulation of Drp1 by CEND1 overexpression was blocked by MG-132 but not CQ (Fig. S6A), which indicates that the degradation of Drp1 by CEND1 was through ubiquitin-proteasome pathway.

By seahorse mitochondrial stress tests, we found that the mitochondrial maximal respiration, ATP production and spare respiratory capacity were significantly impaired in *Cend1*^{-/-} neuron compared with control. These mitochondrial function defects were attenuated by restoration of CEND1 (Fig. 7G) or Drp1 inhibitor Mdivi-1 (Fig. S6B), suggesting that these mitochondria defects induced by CEND1 deficiency due to the upregulation of Drp1 (Fig. S6B). Furthermore, Drp1 overexpression also induced mitochondrial mass damage in N2a cells (Fig. S6C).

CDK5-mediated phosphorylation of CEND1 at S10 residue promotes CEND1 degradation

Overactivation of CDK5 by p25 has been shown to contribute to the pathogenesis of AD [37]. Many phosphorylation targets of CDK5 have been proved to be involved in AD, such as tau and β -secretase [38, 39]. We wondered whether CEND1 was a substrate of CDK5. CDK5 substrates contain an S/TP(X)R/H/K motif, in which S/T could be phosphorylated [40, 41]. According to this motif sequence, a potential phosphorylation site of CDK5 at serine 10 (S10) residue is conserved in species including human, rat, mouse and bos (Fig. 8A). In vitro kinase assays revealed that the S10 residue was the only CDK5 target, given that the phosphorylation

status was completely lost when this residue was mutated into a phosphorylation-resistant alanine (S10A) (Fig. 8B). The mutation of serine 10 to phosphorylation-mimic aspartic acid (S10D) on CEND1 does not change its mitochondrial localization (Fig. S7). By GST pull down assay and endogenous Co-IP, we found that CDK5/p25/CEND1 can bind with each other and form a triple complex in vitro (Fig. 8C–E) and in vivo (Fig. 8F).

We then wondered whether CDK5 may affect CEND1 protein stability through phosphorylation. We first found that CEND1 was increased in CDK5 heterozygous knockout mouse brain compared with controls (Fig. 8G, Fig. S8A). A CDK5 inhibitor (Roscovitine) treatment also increased CEND1 protein level in a dose and time dependent manner in primary neuron (Fig. 8H, Fig. S8B). To gain a better understanding of how CEND1 protein became down-regulated under the influence of CDK5, we modulated protein synthesis and degradation properties of the cells. Treatment with the protein synthesis inhibitor cycloheximide revealed that the rate of CEND1 degradation was significantly faster in cells transfected with CDK5/p25 than CDK5 kinase-dead form (CDK5-KD/p25) (Fig. 8I, J). The degradation rate of phosphorylation-mimic mutant CEND1 (S10D) was also much faster than that of phosphorylation-resistant mutant CEND1 (S10A) (Fig. 8K).

By protein stability assay, we found that the downregulation of CEND1 by CDK5 was blocked by ubiquitin-proteasome inhibitor MG-132 but not autophagy inhibitor CQ (Fig. S8C), which indicates that the degradation of CEND1 by CDK5 is through ubiquitin-proteasome pathway. p35 could be processed to p25 by calpain to over-activate CDK5 [42, 43]. We observed that p35 was cleaved into p25 and CEND1 protein level was decreased when extra calcium (CaCl_2) was added to mouse brain homogenate (Fig. S8D). Glutamate could induce calcium influx to activate calpain in neurons. The protein level of CEND1 was significantly decreased in primary neurons treated with glutamate, and calpain inhibitor MDL8710 could rescue this reduction of CEND1 (Fig. 8L). These data indicated that overactivated CDK5-mediated phosphorylation of CEND1 on S10 residue facilitated its degradation.

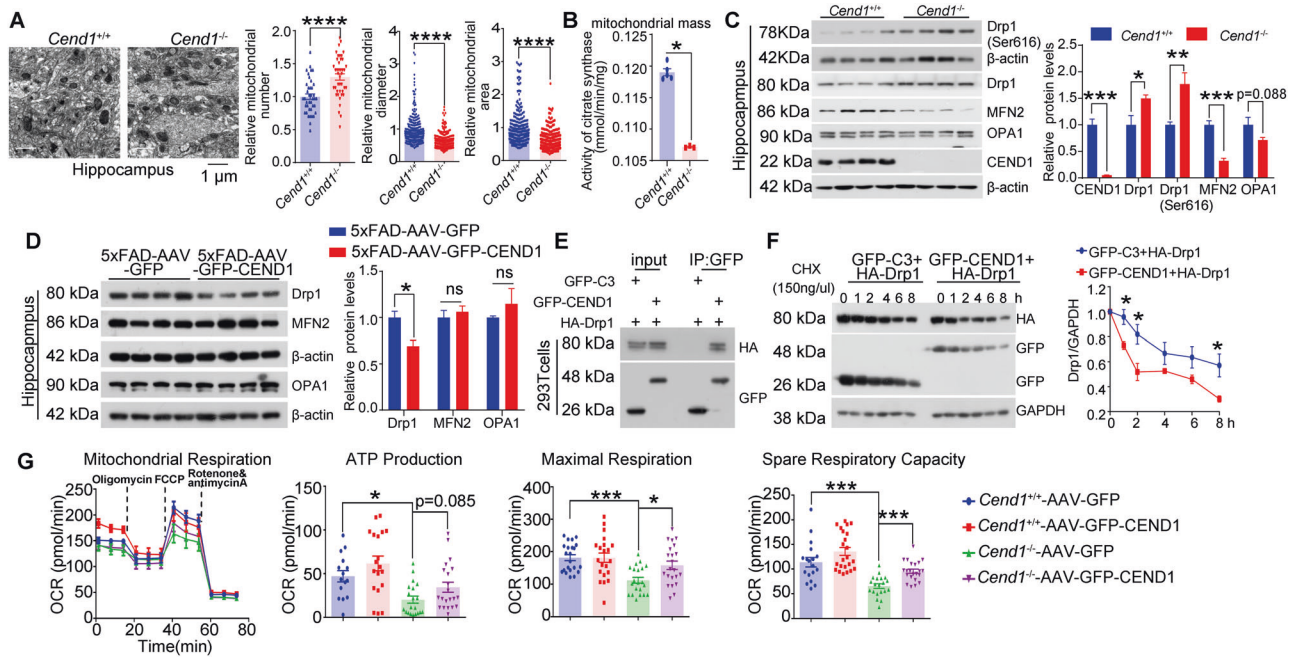


Fig. 7 CEND1 modulates mitochondrial dynamic through regulating Drp1. **A** Hippocampus regions from 6-month-old *Cend1*^{+/+} and *Cend1*^{-/-} mice were subjected to electron microscope imaging and morphometric analysis. Scale bar, 1 μ m. The number, area and diameter of mitochondria were counted. mean \pm SEM, $n \geq 3$, *** $p < 0.001$, by two-tailed Student's *t*-test. **B** Activity of citrate synthase (CS) that reflects mitochondrial mass was determined using total cell lysates of CEND1 knockout primary neuron. The activity of CS was calculated and expressed. mean \pm SEM, $n = 3$, * $p < 0.05$, by two-tailed Student's *t*-test. **C** The hippocampus from WT mice (*Cend1*^{+/+}) and CEND1-deficient mice (*Cend1*^{-/-}) were lysed, then immunoblotted with antibodies against Drp1, Drp1(Ser616), MFN2, CEND1 and β -actin. Quantifications are shown in the right. mean \pm SEM, $n = 4$, * $p < 0.05$, *** $p < 0.001$, by two-tailed Student's *t*-test. **D** The hippocampus from 7-month-old 5xFAD mice injected with AAV-GFP or AAV-GFP-CEND1 were lysed, and immunoblotted with antibodies against Drp1, MFN2, OPA1 and β -actin. Quantifications are shown on the right. mean \pm SEM, $n = 4$ per group, * $p < 0.05$, by two-tailed Student's *t*-test. **E** HEK293T cells were transfected with HA-Drp1 and GFP or GFP-CEND1. GFP proteins were immunoprecipitated and eluates were subjected to Western blotting for HA and GFP. **F** Representative blots showing changes in total HA-CEND1 level in HEK293T cells transfected with HA-Drp1 as well as vector plasmid (GFP-C3) or GFP-CEND1 subjected to CHX treatment for different time courses. Quantification is shown on the right. mean \pm SEM, $n = 4$ per group, * $p < 0.05$, by two-tailed Student's *t*-test. **G** Cortical neurons from indicated mice were cultured in vitro and infected with AAV-GFP or AAV-GFP-CEND1 on DIV7. Basal respiration, proton Leak, ATP production, maximal respiration and spare respiratory capacity were analyzed. mean \pm SEM, $n > 3$ per group, * $P < 0.05$, *** $P < 0.001$, by one-way ANOVA with Tukey post-hoc test.

DISCUSSION

Neurodegenerative diseases, like AD, featured with abnormal mitochondrial function. Mitochondrion is a vital organelle of neurons, which play crucial roles in energy metabolism and cell survival [44, 45]. Functionally damaged mitochondria result in less energy production, more proapoptotic factors production, and more reactive oxygen species (ROS) production, which could lead to neuronal death and impair cognitive function [45–48]. Previous studies indicated that A β induced mitochondrial fragmentation and loss of membrane potential in Alzheimer's disease [49]. Inhibition of excessive mitochondrial fission through different approaches prevented neuronal death and restored cognitive function in AD mice. But the mechanisms for neuronal mitochondrial fusion and fission regulation are not well studied. Here we demonstrated that CEND1 could be a crucial player in maintaining normal mitochondrial morphology and function, and participated in AD pathogenesis. Metabolism change has aroused much more attentions in AD study in recent years. AD patients showed significant decrease of glucose metabolism in the cortex and hippocampus, as showed by PET imaging [50]. Drugs aiming at improving brain metabolic function have shown benefits for AD patients [51]. Our study highlighted the important roles of CEND1 in regulating mitochondrial metabolism, suggesting CEND1 could be a potent therapeutic target for AD treatment.

By synapses isolation, immunofluorescent staining and immunoelectron microscopy analysis, we identified CEND1 specifically locates in presynaptic mitochondria in neurons. Approximately

80% of all axonal mitochondria are located at the pre-synapse and contributes to synaptic functions [52]. A β was also found to bind with mitochondrial proteins (Drp1, VDAC or CypD) at synaptic terminals [53, 54]. Meanwhile, synaptic mitochondria are more vulnerable to stress and damage than the mitochondria in cell body [55]. The damaged synaptic mitochondria cannot supply enough energy for synaptic vesicles transmission, leading to cognitive and learning failure.

CEND1 mediates neuronal cell cycle exit and neuronal differentiation in development neurons, here we explored its new functions in mature neurons and neurodegenerative diseases. Abnormal cell cycle re-entry is associated with many neurodegenerative diseases such as Alzheimer disease (AD) [56, 57]. Accumulating evidence indicate that cell cycle markers (such as cyclin D, CDK4 and Ki67) were significantly elevated in neurons from AD [58–60]. Cell cycle regulation also participates in regulation of mitochondrial fusion/fission and energy production [27, 28]. The atypical cyclin-dependent kinase 5 (CDK5) plays important roles in many cellular functions including cell motility and survival, which directly participate in oxidative stress and mitochondrial morphology in AD pathology. CDK5 is reported to phosphorylate Drp1 at serine616 and S585 [61, 62], which is associated with increased mitochondrial fission. Meanwhile, CDK5 can also phosphorylate HtrA2 at S400 [63] and inactivate peroxiredoxin I and II [64] involving in cell oxidative stress, and triggers mitochondrial fragmentation. Hyperphosphorylation of tau by CDK5 also facilitates mitochondrial dysfunction in

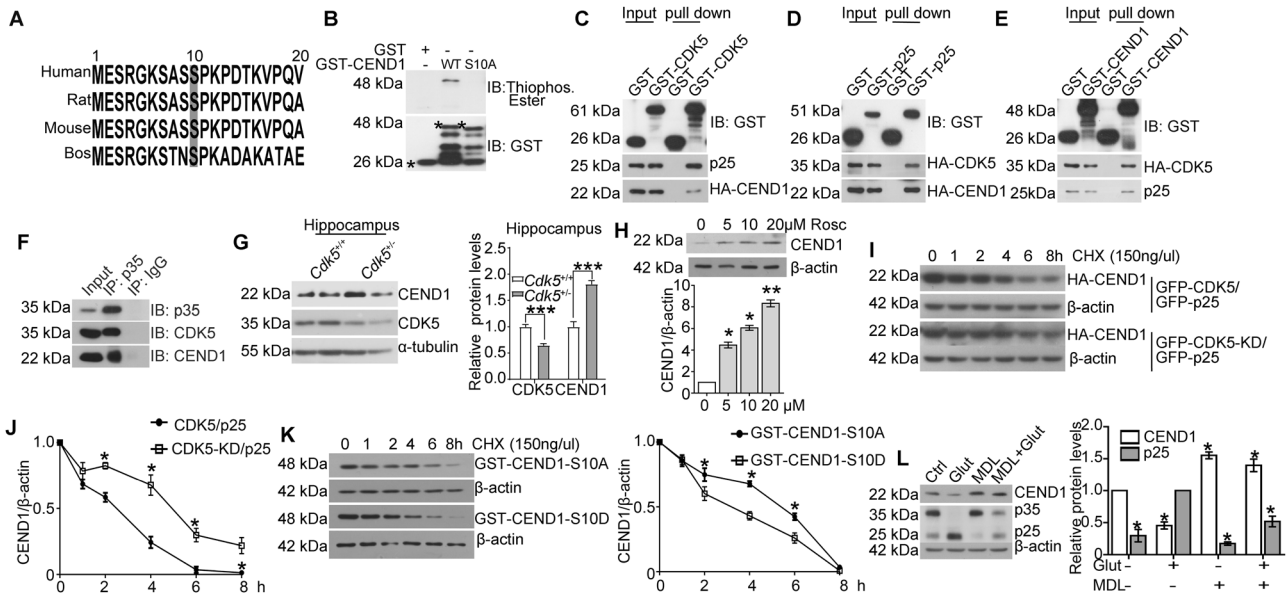


Fig. 8 CDK5-mediated phosphorylation on S10 promotes CEND1 degradation. **A** CEND1 protein sequences of multiple species were aligned. Conserved potential phosphorylation sites are highlighted in black. **B** Representative blots of in vitro CDK5 kinase assays. Phosphorylation on the recombinant GST-CEND1, GST-CEND1 (S10A) or GST tag was tested in vitro in the presence of CDK5/p25 kinase. Reaction products were immunoblotted with an anti-Thiophosphate ester antibody. GST antibody to detect the GST-fusion proteins. **C–E** HEK293T cells were co-transfected with GST-CDK5, p25 and HA-CEND1 (**C**), GST-p25, HA-CDK5 and HA-CEND1 (**D**), or GST-CEND1, HA-CDK5 and p25 (**E**). Cell lysates were subjected to pull-down assays with glutathione-Sepharose beads, and immunoblotted (IB) for the proteins indicated. **F** WT mouse brain lysates were subjected to IP with an antibody against mouse p35 and control immunoglobulin G (IgG), and immunoblotted with antibodies against p35, CDK5 and CEND1. **G** Equal protein amounts of mice hippocampus lysates from *Cdk5*^{+/-} heterozygosity mice and *Cdk5*^{+/+} WT mice were subjected to Western blotting for CEND1, CDK5, and α -tubulin. Quantifications are shown on the right. mean \pm SEM, $n = 4$ per group, *** $p < 0.001$, by two-tailed Student's *t*-test. **H** Representative blots showing changes in CEND1 levels in response to pharmacological inhibition of CDK5 by Roscovitine for different concentrations. β -actin is a loading control. mean \pm SEM, $n = 3$ per group, * $P < 0.05$, ** $P < 0.01$, by one-way ANOVA with Tukey post-hoc test. **I, J** Representative blots showing changes in total HA-CEND1 level in HEK 293T cells transfected with HA-CEND1 as well as CDK/p25 or CDK5-KD/p25 subjected to CHX treatment for different time courses. Quantification is shown in **J**. mean \pm SEM, $n = 3$ per group, * $p < 0.05$, by two-tailed Student's *t*-test. **K** Phosphorylation-mimic mutant CEND1 (S10D) and phosphorylation-dead mutant CEND1 (S10A) were transfected into HEK 293T cells, then treated with CHX for indicated time. Immunoblotted with antibodies against GST and β -actin. mean \pm SEM, $n = 3$ per group, * $p < 0.05$, by two-tailed Student's *t*-test. **L** Mature primary cortical neurons were treated with 100 μ M glutamate for 6 h with or without pretreatment 2 h with 50 μ M MDL28170. Immunoblotted with antibodies against CEND1, p35, p25 and β -actin. mean \pm SEM, $n = 3$ per group, * $P < 0.05$, by one-way ANOVA with Tukey post-hoc test.

neurons [65]. Moreover, inhibition of CDK5 activity can attenuate mitochondrial fission and decrease neuronal apoptosis [66]. We found that overactivated CDK5 phosphorylated CEND1 at serine 10 and promoted its degradation. Reduced CEND1 upregulates expression of Drp1, resulting in aberrant mitochondrial morphology and functions, and cognition impairments. Besides Drp1, we also identified other CEND1 interacting mitochondrial proteins (such as OPA1, VDAC3, ATP5O), which play vital roles in mitochondrial dynamics and OXPHOS [67–69]. CEND1 may also be involved in mitochondrial function by regulating these proteins, which is worth further investigation.

In conclusion, CEND1 locates in presynaptic mitochondria and decreases in AD mice brain. The phosphorylation on S10 residue of CEND1 by CDK5 mediates its degradation. CEND1 deficiency induces Drp1 upregulation and excessive mitochondrial fission, which impairs mitochondrial function and energy production, consequently leading to cognition impairments. Restoration of CEND1 attenuates the cognitive impairments in AD mice (Fig. S9). These results suggested that CEND1 is a key modulator for mitochondria function and targeting CEND1 may therefore provide a therapeutic approach for AD treatment.

DATA AVAILABILITY

Detailed information on the plasmids, sequences of primers, cell culture and other biochemical experiments can be found in supplementary information. For original data, please contact jiezhang@xmu.edu.cn

REFERENCES

- Wang X, Su B, Zheng L, Perry G, Smith MA, Zhu X. The role of abnormal mitochondrial dynamics in the pathogenesis of Alzheimer's disease. *J Neurochem*. 2009;109:153–9.
- Golpich M, Amini E, Mohamed Z, Azman Ali R, Mohamed Ibrahim N, Ahmadiani A. Mitochondrial dysfunction and biogenesis in neurodegenerative diseases: pathogenesis and treatment. *CNS Neurosci Ther*. 2017;23:5–22.
- Benard G, Bellance N, James D, Parrone P, Fernandez H, Letellier T, et al. Mitochondrial bioenergetics and structural network organization. *J Cell Sci*. 2007;120:838–48.
- Frieden M, James D, Castelbou C, Danckaert A, Martinou JC, Demaurex N. Ca(2+) homeostasis during mitochondrial fragmentation and perinuclear clustering induced by hFis1. *J Biol Chem*. 2004;279:22704–14.
- Sugioka R, Shimizu S, Tsujimoto Y. Fzo1, a protein involved in mitochondrial fission, inhibits apoptosis. *J Biol Chem*. 2004;279:52726–34.
- Yu T, Robotham JL, Yoon Y. Increased production of reactive oxygen species in hyperglycemic conditions requires dynamic change of mitochondrial morphology. *Proc Natl Acad Sci USA*. 2006;103:2653–8.
- Onyango IG, Dennis J, Khan SM. Mitochondrial dysfunction in Alzheimer's disease and the rationale for bioenergetics based therapies. *Aging Dis*. 2016;7:201–14.
- Swerdlow RH, Burns JM, Khan SM. The Alzheimer's disease mitochondrial cascade hypothesis: progress and perspectives. *Biochimica et biophysica acta*. 2014;1842:1219–31.
- Singh A, Kukreti R, Saso L, Kukreti S. Oxidative stress: a key modulator in neurodegenerative diseases. *Molecules*. 2019;24:1583.
- Xu LL, Shen Y, Wang X, Wei LF, Wang P, Yang H, et al. Mitochondrial dynamics changes with age in an APPsw/PS1dE9 mouse model of Alzheimer's disease. *Neuroreport* 2017;28:222–8.
- Hu C, Huang Y, Li L. Drp1-dependent mitochondrial fission plays critical roles in physiological and pathological progresses in mammals. *Int J of mol sci*. 2017;18:144.

12. Kandimalla R, Reddy PH. Multiple faces of dynamin-related protein 1 and its role in Alzheimer's disease pathogenesis. *Biochimica et biophysica acta*. 2016;1862: 814–28.
13. Nakamura T, Cieplak P, Cho DH, Godzik A, Lipton SA. S-nitrosylation of Drp1 links excessive mitochondrial fission to neuronal injury in neurodegeneration. *Mitochondrion* 2010;10:573–8.
14. Chang CR, Blackstone C. Cyclic AMP-dependent protein kinase phosphorylation of Drp1 regulates its GTPase activity and mitochondrial morphology. *J Biol Chem*. 2007;282:21583–7.
15. Zaja I, Bai X, Liu Y, Kikuchi C, Dosenovic S, Yan Y, et al. Cdk1, PKCdelta and calcineurin-mediated Drp1 pathway contributes to mitochondrial fission-induced cardiomyocyte death. *Biochemical biophysical Res Commun*. 2014;453:710–21.
16. Huang J, Xie P, Dong Y, An W. Inhibition of Drp1 SUMOylation by ALR protects the liver from ischemia-reperfusion injury. *Cell Death Differ*. 2021;28:1174–92.
17. Kashatus JA, Nascimento A, Myers LJ, Sher A, Byrne FL, Hoehn KL, et al. Erk2 phosphorylation of Drp1 promotes mitochondrial fission and MAPK-driven tumor growth. *Mol Cell*. 2015;57:537–51.
18. Taguchi N, Ishihara N, Jofuku A, Oka T, Mihara K. Mitotic phosphorylation of dynamin-related GTPase Drp1 participates in mitochondrial fission. *J Biol Chem*. 2007;282:11521–9.
19. Nakamura N, Kimura Y, Tokuda M, Honda S, Hirose S. MARCH-V is a novel mitofusin 2- and Drp1-binding protein able to change mitochondrial morphology. *EMBO Rep*. 2006;7:1019–22.
20. Patsavoudi E, Merkouri E, Thomaidou D, Sandillon F, Alonso G, Matsas R. Characterization and localization of the BM88 antigen in the developing and adult rat brain. *J Neurosci Res*. 1995;40:506–18.
21. Gaitanou M, Segklia K, Matsas R. Cend1, a story with many tales: from regulation of cell cycle progression/exit of neural stem cells to brain structure and function. *Stem Cells Int*. 2019;2019:2054783.
22. Politis PK, Makri G, Thomaidou D, Geissen M, Rohrer H, Matsas R. BM88/CEND1 coordinates cell cycle exit and differentiation of neuronal precursors. *Proc Natl Acad Sci USA*. 2007;104:17861–6.
23. Georgopoulou N, Hurel C, Politis PK, Gaitanou M, Matsas R, Thomaidou D. BM88 is a dual function molecule inducing cell cycle exit and neuronal differentiation of neuroblastoma cells via cyclin D1 down-regulation and retinoblastoma protein hypophosphorylation. *J Biol Chem*. 2006;281:33606–20.
24. Katsimpardi L, Gaitanou M, Malnou CE, Lledo PM, Charneau P, Matsas R, et al. BM88/Cend1 expression levels are critical for proliferation and differentiation of subventricular zone-derived neural precursor cells. *Stem Cells*. 2008;26:1796–807.
25. Makri G, Lavdas AA, Katsimpardi L, Charneau P, Thomaidou D, Matsas R. Transplantation of embryonic neural stem/precursor cells overexpressing BM88/Cend1 enhances the generation of neuronal cells in the injured mouse cortex. *Stem Cells*. 2010;28:127–39.
26. Sergaki MC, Guillemot F, Matsas R. Impaired cerebellar development and deficits in motor coordination in mice lacking the neuronal protein BM88/Cend1. *Mol Cell Neurosci*. 2010;44:15–29.
27. Horbay R, Bilyy R. Mitochondrial dynamics during cell cycling. *Apoptosis* 2016;21:1327–35.
28. Lopez-Mejia IC, Fajas L. Cell cycle regulation of mitochondrial function. *Curr Opin Cell Biol*. 2015;33:19–25.
29. Lu TT, Wan C, Yang W, Cai Z. Role of Cdk5 in amyloid-beta pathology of Alzheimer's disease. *Curr Alzheimer Res*. 2019;16:1206–15.
30. Liu SL, Wang C, Jiang T, Tan L, Xing A, Yu JT. The role of Cdk5 in Alzheimer's disease. *Mol Neurobiol*. 2016;53:4328–42.
31. Meuer K, Suppanz IE, Lingor P, Planchamp V, Gorick B, Fichtner L, et al. Cyclin-dependent kinase 5 is an upstream regulator of mitochondrial fission during neuronal apoptosis. *Cell Death Differ*. 2007;14:651–61.
32. Cherubini M, Puigdemilliv M, Alberch J, Gines S. Cdk5-mediated mitochondrial fission: a key player in dopaminergic toxicity in Huntington's disease. *Biochimica et biophysica acta*. 2015;1852:2145–60.
33. Yang SH, Huang CY, Hsieh CY, Chuang JI. CDK4 and CDK5 inhibition have comparable mild hypothermia effects in preventing Drp1-dependent mitochondrial fission and neuron death induced by MPP(+). *Mol Neurobiol*. 2020;57: 4090–105.
34. Guo MY, Shang L, Hu YY, Jiang LP, Wan YY, Zhou QQ, et al. The role of Cdk5-mediated Drp1 phosphorylation in Abeta1-42 induced mitochondrial fission and neuronal apoptosis. *J Cell Biochem*. 2018;119:4815–25.
35. Wang H, Dey KK, Chen PC, Li Y, Niu M, Cho JH, et al. Integrated analysis of ultra-deep proteomes in cortex, cerebrospinal fluid and serum reveals a mitochondrial signature in Alzheimer's disease. *Mol Neurodegener*. 2020;15:43.
36. Pereira PA, Tomas JF, Queiroz JA, Figueiras AR, Sousa F. Recombinant pre-miR-29b for Alzheimer's disease therapeutics. *Sci Rep*. 2016;6:19946.
37. Seo J, Kritskiy O, Watson LA, Barker SJ, Dey D, Raja WK, et al. Inhibition of p25/CDK5 attenuates tauopathy in mouse and iPSC models of frontotemporal dementia. *J Neurosci: Off J Soc Neurosci*. 2017;37:9917–24.
38. Kimura T, Ishiguro K, Hisanaga S. Physiological and pathological phosphorylation of tau by Cdk5. *Front Mol Neurosci*. 2014;7:65.
39. Wen Y, Yu WH, Maloney B, Bailey J, Ma J, Marie I, et al. Transcriptional regulation of beta-secretase by p25/cdk5 leads to enhanced amyloidogenic processing. *Neuron* 2008;57:680–90.
40. Matsuura I, Bondarenko VA, Maeda T, Kachi S, Yamazaki M, Usukura J, et al. Phosphorylation by cyclin-dependent protein kinase 5 of the regulatory subunit of retinal cGMP phosphodiesterase. I. Identification of the kinase and its role in the turnover of phosphodiesterase in vitro. *J Biol Chem*. 2000;275:32950–7.
41. Maccioni RB, Otth C, Concha II, Munoz JP. The protein kinase Cdk5. Structural aspects, roles in neurogenesis and involvement in Alzheimer's pathology. *Eur J Biochem*. 2001;268:1518–27.
42. Zhang H, Chang L, Zhang H, Nie J, Zhang Z, Yang X, et al. Calpain-2/p35-p25/CDK5 pathway is involved in the neuronal apoptosis induced by polybrominated diphenyl ether-153. *Toxicol Lett*. 2017;277:41–53.
43. Camins A, Verdaguer E, Folch J, Canudas AM, Pallas M. The role of CDK5/P25 formation/inhibition in neurodegeneration. *Drug N. Perspect*. 2006;19:453–60.
44. Sims NR, Finegan JM, Blass JP, Bowen DM, Neary D. Mitochondrial function in brain tissue in primary degenerative dementia. *Brain Res*. 1987;436:30–8.
45. Hirai K, Aliev G, Nunomura A, Fujioka H, Russell RL, Atwood CS, et al. Mitochondrial abnormalities in Alzheimer's disease. *J Neurosci: Off J Soc Neurosci*. 2001;21:3017–23.
46. de la Monte SM, Luong T, Neely TR, Robinson D, Wands JR. Mitochondrial DNA damage as a mechanism of cell loss in Alzheimer's disease. *Lab Invest; a J Tech methods Pathol*. 2000;80:1323–35.
47. Coskun PE, Beal MF, Wallace DC. Alzheimer's brains harbor somatic mtDNA control-region mutations that suppress mitochondrial transcription and replication. *Proc Natl Acad Sci USA*. 2004;101:10726–31.
48. Cai Q, Tammineni P. Alterations in mitochondrial quality control in Alzheimer's disease. *Front Cell Neurosci*. 2016;10:24.
49. Han J, Park H, Maharana C, Gwon AR, Park J, Baek SH, et al. Alzheimer's disease-causing presenilin-1 mutations have deleterious effects on mitochondrial function. *Theranostics* 2021;11:8855–73.
50. Valotassiou V, Malamitsi J, Papatrifiantayllou J, Dardiotis E, Tsougos I, Psimidias D, et al. SPECT and PET imaging in Alzheimer's disease. *Ann Nucl Med*. 2018;32: 583–93.
51. Vargas-Soria M, Carranza-Naval MJ, Del Marco A, Garcia-Alloza M. Role of liraglutide in Alzheimer's disease pathology. *Alzheimer's Res Ther*. 2021;13:112.
52. Smith HL, Bourne JN, Cao G, Chirillo MA, Ostroff LE, Watson DJ, et al. Mitochondrial support of persistent presynaptic vesicle mobilization with age-dependent synaptic growth after LTP. *Elife*. 2016;5:e15275.
53. Reddy PH, Oliver DM. Amyloid beta and phosphorylated tau-induced defective autophagy and mitophagy in Alzheimer's disease. *Cells*. 2019;8:488.
54. Du H, Guo L, Fang F, Chen D, Sosunov AA, McKhann GM, et al. Cyclophilin D deficiency attenuates mitochondrial and neuronal perturbation and ameliorates learning and memory in Alzheimer's disease. *Nat Med*. 2008;14:1097–105.
55. Pradeepkiran JA, Reddy PH. Defective mitophagy in Alzheimer's disease. *Ageing Res Rev*. 2020;64:101191.
56. Moh C, Kubiak JZ, Bajic VP, Zhu X, Smith MA, Lee HG. Cell cycle deregulation in the neurons of Alzheimer's disease. *Results Probl Cell Differ*. 2011;53:565–76.
57. Zhu X, Lee HG, Perry G, Smith MA. Alzheimer disease, the two-hit hypothesis: an update. *Biochimica et biophysica acta*. 2007;1772:494–502.
58. Czapski GA, Cieslik M, Bialopiotrowicz E, Lukiw WJ, Strosznajder JB. Down-regulation of cyclin D2 in amyloid beta toxicity, inflammation, and Alzheimer's disease. *PLoS one*. 2021;16:e0259740.
59. McShea A, Harris PL, Webster KR, Wahl AF, Smith MA. Abnormal expression of the cell cycle regulators P16 and CDK4 in Alzheimer's disease. *Am J Pathol*. 1997;150:1933–9.
60. Vincent I, Rosado M, Davies P. Mitotic mechanisms in Alzheimer's disease? *J Cell Biol*. 1996;132:413–25.
61. Chen C, Peng X, Tang J, Hu Z, Tan J, Zeng L. CDK5 inhibition protects against OGD-induced mitochondrial fragmentation and apoptosis through regulation of Drp1S616 phosphorylation. *Life Sci*. 2021;269:119062.
62. Jahani-Asl A, Huang E, Irrcher I, Rashidian J, Ishihara N, Lagace DC, et al. CDK5 phosphorylates DRP1 and drives mitochondrial defects in NMDA-induced neuronal death. *Hum Mol Genet*. 2015;24:4573–83.
63. Fitzgerald JC, Camprubi MD, Dunn L, Wu HC, Ip NY, Kruger R, et al. Phosphorylation of HtrA2 by cyclin-dependent kinase-5 is important for mitochondrial function. *Cell Death Differ*. 2012;19:257–66.
64. Park J, Choi H, Min JS, Kim B, Lee SR, Yun JW, et al. Loss of mitofusin 2 links beta-amyloid-mediated mitochondrial fragmentation and Cdk5-induced oxidative stress in neuron cells. *J Neurochemistry*. 2015;132:687–702.
65. Quintanilla RA, von Bernhardi R, Godoy JA, Inestrosa NC, Johnson GV. Phosphorylated tau potentiates Abeta-induced mitochondrial damage in mature neurons. *Neurobiol Dis*. 2014;71:260–9.

66. Weishaupt JH, Kussmaul L, Grottsch P, Heckel A, Rohde G, Romig H, et al. Inhibition of CDK5 is protective in necrotic and apoptotic paradigms of neuronal cell death and prevents mitochondrial dysfunction. *Mol Cell Neurosci.* 2003; 24:489–502.
67. Gao S, Hu J. Mitochondrial fusion: the machineries in and out. *Trends Cell Biol.* 2021;31:62–74.
68. Reina S, Guarino F, Magri A, De Pinto V. VDAC3 as a potential marker of mitochondrial status is involved in cancer and pathology. *Front Oncol.* 2016;6:264.
69. Yang W, Nagasawa K, Munch C, Xu Y, Satterstrom K, Jeong S, et al. Mitochondrial sirtuin network reveals dynamic SIRT3-dependent deacetylation in response to membrane depolarization. *Cell* 2016;167:985–1000. e21.

ACKNOWLEDGEMENTS

We thank the excellent technical assistance provided by the core facility of biomedical sciences in Xiamen University.

AUTHOR CONTRIBUTIONS

WX, KZ, GC, and JL performed the animal experiments; WX, DG, QK, HW, TZ, HL, and LY performed cellular and biochemical assays; WX, DG, WG, and JZ wrote the manuscript. ZC, and LL discussed and edited the manuscript. JZ supervised the project. All authors reviewed and gave final approval to the manuscript.

FUNDING

This work was supported by the National Natural Science Foundation of China (Grant: 81925010, 91849205, U1905207 and 92149303 to JZ; 81902423 to DG);

The National Key Research and Development Program of China (Grant: 2021YFA1101402 to JZ).

COMPETING INTERESTS

The authors declare no competing interests.

ETHICS APPROVAL

Our studies did not include human participants or human tissue. The animal studies were approved by ethics Institutional Animal Care and Use Committee at Xiamen University.

ADDITIONAL INFORMATION

Supplementary information The online version contains supplementary material available at <https://doi.org/10.1038/s41418-022-01027-7>.

Correspondence and requests for materials should be addressed to Weiwei Gao or Jie Zhang.

Reprints and permission information is available at <http://www.nature.com/reprints>

Publisher's note Springer Nature remains neutral with regard to jurisdictional claims in published maps and institutional affiliations.